A Broadband Low-Noise-Amplifier

Luca Daniel and Manolis Terrovitis
May 1999

Department of Electrical Engineering & Computer Sciences
University of California, Berkeley CA 94720

Abstract

This report describes the design of a two-stage broadband low-noise-amplifier (LNA) for the frequency range from 3 GHz to 9 GHz, using GaAs MESFETs with an f_t of 20 GHz. The passive components were implemented with microstrips. In the frequency band of operation, the achieved noise figure (NF) is within 0.5 dB from the minimum NF of a single transistor, the power gain is 15 dB, flat within 1 dB, and the maximum input VSWR is lower than 3.

1. Introduction

Broadband LNAs find application in communication systems and instrumentation equipment. Since the LNA is the first circuit block in a receiver chain, its noise performance dominates the system sensitivity. The primary objective of this work is to achieve low noise figure and flat gain over the wide frequency range of operation. Other considerations are low input voltage standing wave ratio (VSWR), and large range of source and load impedances for which the amplifier remains stable.

While minimum noise figure in narrow band amplifiers can be obtained with a single-frequency impedance matching network, achieving close-to-minimum noise figure across a wide frequency band is significantly more complicated. For this purpose, a resonance matching network is employed at the input, to track with frequency the optimal source impedance which results in the minimum noise figure.

Inductive degeneration has been used in narrow-band amplifiers to achieve simultaneous matching for high gain and low noise [1]. Similarly, using inductive degeneration in our wide-band application we achieve close to minimum noise figure and reduced input VSWR.

The minimum noise figure of a GaAs MESFET is shown to increase with frequency (see Fig. 3 below). When designing a broadband LNA one can minimize the noise figure at every frequency point, or require that the noise figure is lower than some upper bound. The second approach allows the noise figure to be higher than the minimum at low frequencies and gives a wider band of operation. Both types of wide-band LNAs find applications, but the first option was chosen for this design.

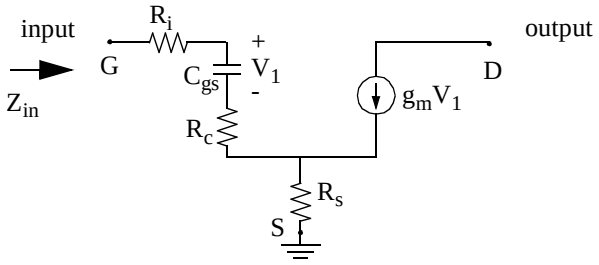

Fig. 1. Representation of a GaAs MESFET common-source amplifier, using a simple small-signal model for the transistor.

2. Common-Source Amplifiers - Background

A popular topology for the implementation of LNAs is the common-source configuration. Such an amplifier employing a GaAs MESFET transistor is shown in Fig. 1, where a simplified small-signal transistor model has been used. The input impedance and the noise performance of this amplifier will be reviewed briefly in this section.

2.1 Input impedance

One can show that the input impedance of the amplifier of Fig. 1 is given by

$$Z_{in} = R_i + R_c + R_s + \frac{1 + g_m R_s}{j\omega C_{gs}} \qquad (1)$$

The gain of the amplifier is maximized, and the reflections to the generator are minimized, when a lossless input matching network is employed which transforms the 50 Ω line impedance to the conjugate of Z_{in}.

2.2 Noise performance

A noisy two-port can be represented with the equivalent input voltage and current noise generators preceding the noiseless network, as shown in Fig. 2. The two generators are in general correlated, and for this reason the voltage noise generator is partitioned into two voltage sources, one uncorrelated and one fully correlated with the current generator. Let us denote the current noise generator with i_n, the uncorrelated part of the voltage generator with v_n and its correlated part with $i_n Z_{cor}$, where $Z_{cor}=R_{cor}+jX_{cor}$ is called the correlation impedance. Also let G_n

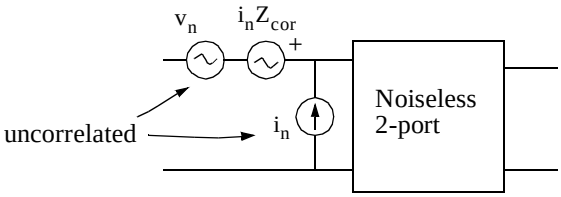

Fig. 2. Representation of a noisy two-port with correlated input noise generators.

and R_n be related with the power spectral densities of i_n and v_n as follows

$$\overline{i_n^2}/\Delta f = 4kTG_n \tag{2}$$

$$\overline{v_n^2}/\Delta f = 4kTR_n \tag{3}$$

where k is Boltzman's constant and T is the absolute temperature. It can be shown [3] that the source (or generator) impedance $Z_{g,opt}=R_{g,opt}+ jX_{g,opt}$ needed to achieve the minimum noise figure is

$$R_{g,\,opt} = \sqrt{\frac{R_n}{G_n} + R_{cor}^2} \tag{4}$$

$$X_{g,\,opt} = -X_{cor} \tag{5}$$

and the minimum noise figure is given by

$$F_{min} = 1 + 2G_nR_{cor} + 2\sqrt{R_nG_n + (G_nR_{cor})^2}\ . \tag{6}$$

For a different source impedance $Z_g=R_g+jX_g$, the noise figure is

$$F = F_{min} + \frac{G_n}{R_g}\cdot\left|Z_g - Z_{g,\,opt}\right|^2\ . \tag{7}$$

For a GaAs MESFET transistor in the common source configuration, a theoretical analysis [4] in which velocity saturation effects are taken into account, gives the following expressions for the noise parameters R_n, G_n, and Z_{cor}

$$R_n = (R_s + R_i)\frac{T_a}{T_o} + K_r\frac{(1+\omega^2C_{gs}^2R_c^2)}{g_m} \tag{8}$$

$$G_n = K_g\frac{\omega^2C_{gs}^2}{g_m} \tag{9}$$

$$Z_{cor} = R_s + R_i + K_c\left(R_c + \frac{1}{j\omega C_{gs}}\right) \tag{10}$$

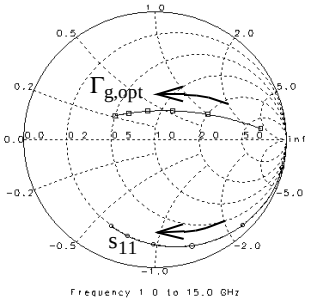

(a)

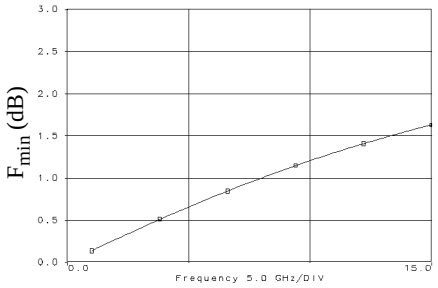

(b)

Fig. 3. (a) Optimal source reflection coefficient $\Gamma_{g,opt}$ which results in minimum noise figure, and s_{11}. The arrows show the direction of frequency increase. (b) minimum noise figure for a GaAs MESFET in common-source configuration.

where the quantities R_i, R_c, R_s, C_{gs} and g_m are defined in Fig. 1. The coefficients K_c, K_g and K_r depend on bias, but are constant with frequency. Parameter T_a is the temperature of the FET, while T_o is some reference temperature for the above coefficients, usually 290^o K.

The optimal source reflection coefficient which results in the minimum noise figure, together with s_{11} versus frequency as obtained from simulation is shown in Fig. 3(a), and the minimum noise figure is shown in Fig. 3(b).

3. Broadband Impedance Matching

From equations (5) and (10), we observe that for a broadband matching of the optimal source impedance which results in the minimum noise figure we need a circuit that approximately imitates the behavior of a negative capacitor. A negative capacitor is also needed for the broadband conjugate matching of the amplifier input impedance, as can be seen from equation (1). In Fig. 3(a), we observe that the input reflection coefficient s_{11} moves clockwise with frequency and therefore the optimal for gain source reflection coefficient which is the conjugate of s_{11} moves counterclockwise. Similarly the optimal source reflection coefficient which results in minimum noise figure also moves counterclockwise with frequency.

However, counterclockwise movement on the Smith chart cannot be achieved with a passive matching network without resonances. Foster's theorem [2] states that the reactance seen from the port of any passive lossless network has a positive derivative with frequency and therefore it is an increasing function of frequency. One can easily verify the above for a single capacitor or inductor, or a series or parallel LC circuit. A similar behavior is observed for the imaginary part of the impedance seen from the port of any lossy passive network without resonances, or even with resonances if we observe the network at frequencies far away from the resonance frequencies. On the Smith chart increasing reactance corresponds to clockwise movement as frequency increases. In other words, the imaginary part of the port impedance of a passive network without resonances can only approximate a positive capacitor or a positive inductor.

3.1 Broadband matching with a resonant circuit

A lossy resonant circuit can imitate the behavior of a negative capacitor or inductor in the frequency range close to the resonance. An example of such a circuit is shown in Fig. 4. On the Smith chart of Fig. 5(a), it can be seen that the trajectory of the reflection coefficient for frequency values close to resonance forms a close loop. For part of this loop the reflection coefficient moves counterclockwise and can approximately track the optimal source impedance which results in minimum noise figure. The real and imaginary part of this optimal source impedance, compared with the impedance achieved with the network of Fig. 4 are shown in Fig. 5(b) and Fig. 5(c), where good agreement is observed in a quite large frequency band. The use of an optimization routine is essential for the fine tuning of the component values.

Since resistors are undesirable because they introduce noise and signal power loss, the real impedance of the 50 Ω input line can be used instead, to realize the resistor of the circuit of Fig. 4. In general, the desirable value for the resistance of this network is different than 50 Ω, but a lossless Chebyshev of Binomial multisection transformer can be used to achieve a broadband impedance transformation of the 50 Ω to the desirable value.

4. Inductive Degeneration

Source degeneration introduces negative series feedback and reduces the gain of the amplifier. However, it provides one more degree of freedom with which one can affect the input impedance of the amplifier, the minimum noise figure, and the optimal source impedance which results in minimum noise figure. Inductive degeneration is of particular interest because it does not introduce noise.

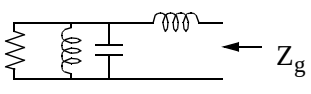

Fig. 4. A resonant circuit capable of approximating a negative capacitor in the frequency range close to the resonance frequency

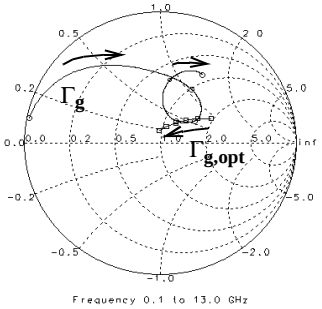

(a)

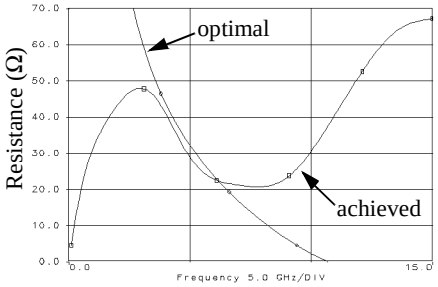

(b)

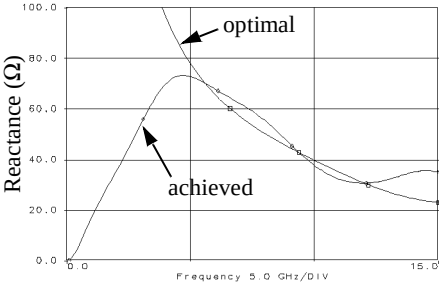

(c)

Fig. 5. Optimal source impedance which results in minimum noise figure and impedance achieved with the resonance network of Fig. 4. (a) on the Smith chart, (b) real part, and (c) imaginary part. The arrows on the Smith chart show the direction of frequency increase.

4.1 Effect on Input Impedance

If inductive degeneration L_s is used in the common source amplifier of Fig. 1, the input impedance becomes

$$Z_{in} = R_i + R_c + R_s + \frac{g_m L_s}{C_{gs}} + j\omega L_s + \frac{1 + g_m R_s}{j\omega C_{gs}} \qquad (11)$$

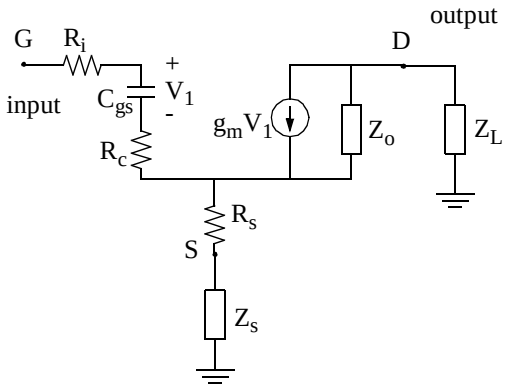

Fig. 6. A common-source amplifier with degeneration, including the output device impedance and a load.

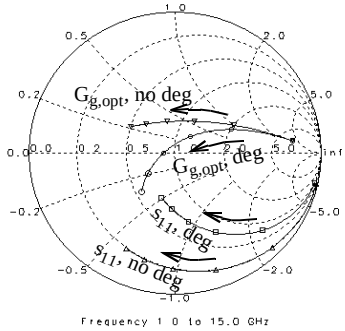

Fig. 7. Optimal reflection coefficient $\Gamma_{g,opt}$ which results in minimum noise figure and reflection coefficient s_{11}, with and without inductive degeneration. The arrows show the direction of frequency increase.

Using a more detailed model for the transistor which includes the device output impedance Z_o, the input impedance can be found to be

$$Z_{in} = R_i + R_c + \frac{1}{j\omega C_{gs}} + \left(1 + \frac{g_m}{j\omega C_{gs}} \cdot \frac{Z_o}{Z_o + Z_L}\right) \cdot ((R_s + Z_s)//(Z_o + Z_L)) \quad (12)$$

where Z_L and Z_s are the load and degeneration impedances respectively.

We conclude that inductive degeneration provides a way to modify the input impedance. Besides, it increases the real part of the input impedance and it improves the stability of the amplifier.

4.2 Effect on the optimal for noise source impedance and the minimum noise figure

Let G_n', R_n' and Z_{cor}' denote the parameters that describe the equivalent input noise generators of the amplifier with source degeneration Z_s. Analysis using the simple small-signal model of Fig. 1, shows that these parameters can be expressed in terms of the corresponding parameters of the undegenerated amplifier as follows

$$G_n' = G_n \quad (13)$$

$$R_n' = R_n \quad (14)$$

$$Z_{cor}' = Z_{cor} + Z_s \quad (15)$$

The effect of inductive degeneration on the input impedance and the optimal source impedance which results in the minimum noise figure is shown in Fig. 7. In [1] it is shown that by varying the degeneration and load impedances it is possible to make the optimal for noise source impedance coincide with the conjugate of the input impedance of the amplifier in a narrow frequency band and therefore achieve simultaneous matching for noise and gain performance while eliminating the reflections from the input port.

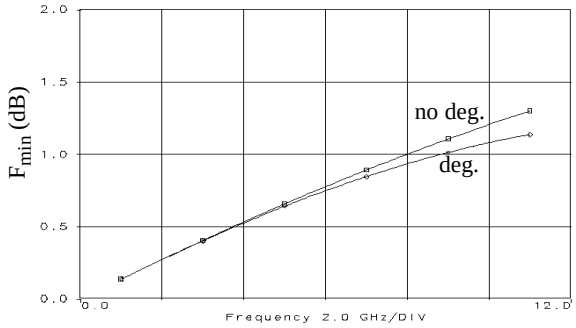

Fig. 8. Minimum noise figure of a common-source single transistor amplifier, with and without inductive degeneration.

With inductive degeneration, from (15) which assumes the simple model of Fig. 1, the real part of the correlation impedance remains the same as without degeneration and (6) predicts that the minimum noise figure remains the same. However, simulation with a more elaborate model including the output impedance of the device and a load, shows that inductive degeneration is also beneficial because it reduces the minimum noise figure of the amplifier. The minimum noise figure for a single-transistor common source amplifier with and without degeneration is shown in Fig. 8.

5. Design with Ideal Passive Components

The two stage LNA design with ideal passive components is shown in Fig. 9. The input matching network discussed in section 3.1 was used. A Chebyshev two-section transformer was used to transform the 50 Ω to about 80 Ω that our circuit requires. The

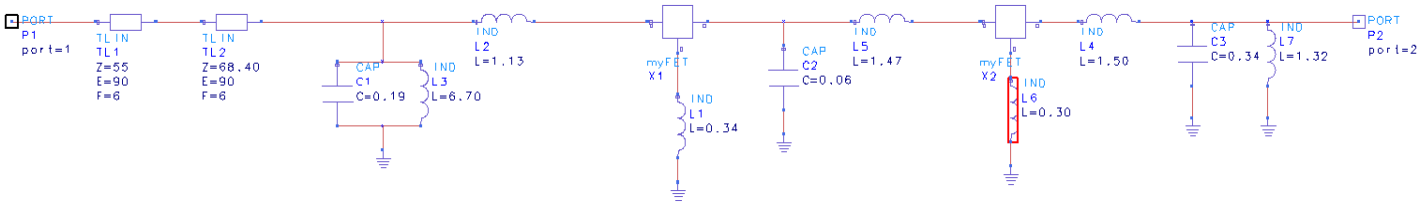

Fig. 9. The two-stage broadband LNA design with ideal passive components.

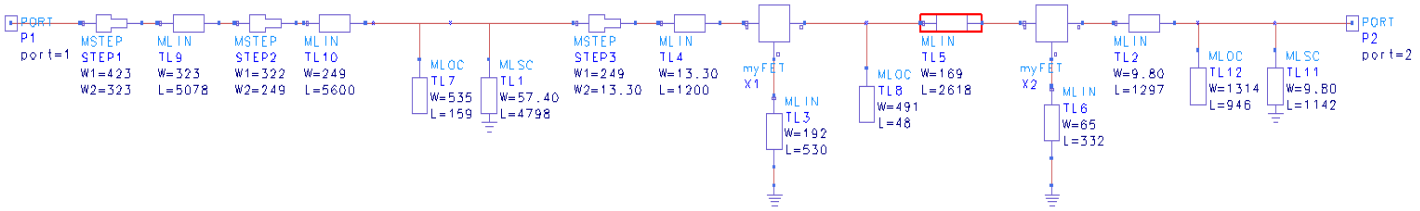

Fig. 10. The LNA design, with the passive components implemented with microstrips.

second stage was employed to provide a high gain. Inductive degeneration was used in both stages to reduce the minimum noise figure, to help the stability and to lower the input reflections. As can be seen in Fig. 7, inductive degeneration can bring the conjugate of the input reflection coefficient closer to the optimal reflection coefficient which results in minimum noise figure, and therefore achieve reduced input VSWR. The interstage and the output matching networks were designed to provide a flat gain response in the frequency range of operation. The EEsof microwave design package from Hewlett Packard was used for the simulation. The GaAs MESFET transistors used have an f_t of 20 GHz, and the transistor model used in the simulations is described in the appendix. The fine tuning of the component values was determined with the aid the of optimizer of the CAD tool. The component values can be read from the schematic.

6. Microstrip Implementation

The circuit of Fig. 9 was implemented with microstrips as shown in Fig. 10, and simulated. The shunt capacitors were replaced by open stubs of low characteristic impedance, while the shunt inductors were replaced by shorted stubs. In order to avoid changing the behavior of these components at high frequencies, the length of these transmission line sections was kept shorter than $\lambda/8$ at the highest frequency of operation. The series inductors were implemented with narrow section high impedance microstrip. Some of these long and narrow lossy microstrips were found to contribute significantly to the noise because of their high resistivity. Wider and longer microstrips were employed because they were found to introduce lower resistance and noise. Their length slightly exceeded the $\lambda/8$ limit at the highest frequency of operation, but not significant degradation in the performance was observed. The relative dielectric constant of the substrate used was ε_r=9, the substrate thickness was h=400 μm, and the metal thickness was t=5 μm. The S-matrices of the discontinuities in the width of the transmission lines were included in the simulation, but they were found to have a negligible effect in the frequency range of interest.

The design was fine tuned again using the optimizer of the CAD tool, and the component values can be read from the schematic. The performance of the amplifier implemented with microstrips compared with the performance of the circuit realized with ideal passive components is shown in Fig. 11. The minimum and achieved noise figure of the two implementations is shown in Fig. 11(a). Since as we mentioned above practical transmission lines are lossy and contribute noise, the noise figure of the system with microstrips is higher than this of the system with ideal components. The gain, shown in Fig. 11(b), is equal to 15 dB flat within 1 dB for both implementations. The VSWR, shown in Fig. 11(c) remains below 3 for the microstrip implementation, while it is higher for the ideal component circuit. If these reflections are detrimental to the source, one can use a directional coupler at the input and drive the reflections to a matched termination.

7. Stability

The microstrip amplifier implementation was tested for stability in the frequency range from 0 to 60 GHz. A sufficient condition for the stability of the amplifier is that the impedance seen at the input and at the output of every stage has a positive real part [5]. Positive real part of the impedance is equivalent to a reflection coefficient with magnitude lower than one. It is worth noticing that if a lossless matching network precedes a network port, for energy conservation reasons the real part of the impedance will have the same sign before and after the matching network. Therefore the output stability circles are not affected by

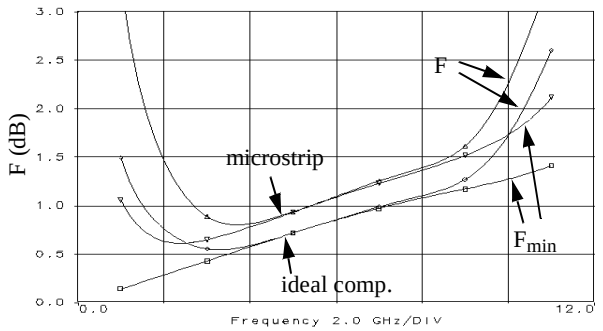

(a)

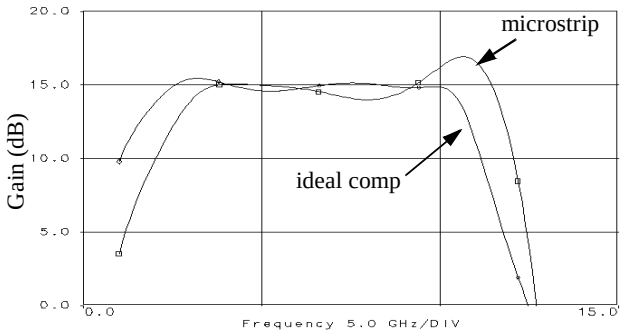

(b)

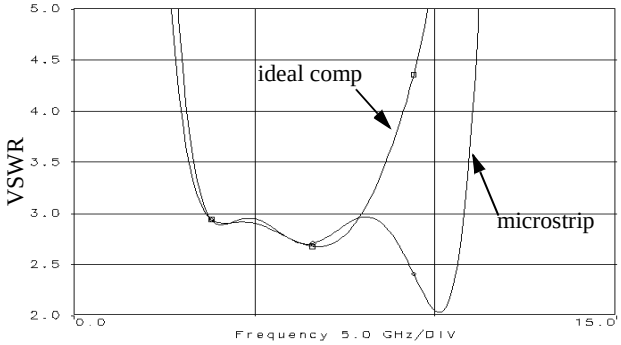

(c)

Fig. 11. Performance of the broadband LNA, for the ideal passive component and the microstrip implementation. (a) NF and NFmin, (b) gain, (c) VSWR.

such a lossless matching network at the input, and similarly the input stability circles are not affected by a lossless matching network at the output.

When the load impedance is equal to the nominal 50 Ω, the magnitude of the reflection coefficient seen at the input of the first and second stage is shown in Fig. 12(a) and is indeed lower than one. To find the region of load impedances that give a reflection coefficient with magnitude lower than one at the input

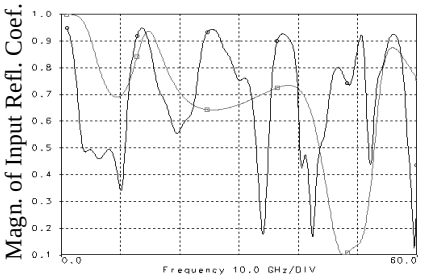

(a)

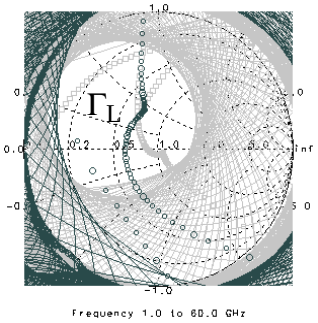

(b)

Fig. 12. (a) Reflection coefficient at the input of the first and second stage when a 50 Ω load is connected at the output. (b) The output stability circles define the region of the load reflection coefficient Γ_L for which the amplifier remains stable. The small squares are the center of the circles.

of the first and second stage, we show the corresponding output stability circles in Fig. 12(b), from 0 to 60 GHz. Since the center of the Smith chart has been verified to belong to the stable region, the wide area that is not covered by the circle lines and that contains the center corresponds to load values that lead to stability. A load impedance located outside this area for some frequencies does not necessarily mean instability because for these frequencies it can remain in the stable side of the stability circles. However, if the load impedance remain in the region shown in Fig. 12(b) for all frequencies, stability is guaranteed.

The same test was performed for the reflection coefficient at the output of the first and second stage. Fig. 13(a) shows the magnitude of the reflection coefficient when the source impedance is equal to 50 Ω, and Fig. 13(b) shows the corresponding input stability circles. Again, the wide area that is not covered by the circle lines and contains the center corresponds to source impedances for which the amplifier is stable

8. Conclusions

A two stage broadband LNA has been designed and implemented in microstrip technology. A resonant circuit was employed at the input to achieve a broadband matching of the generator impedance to the optimal source impedance which results in minimum noise figure. Inductive degeneration was

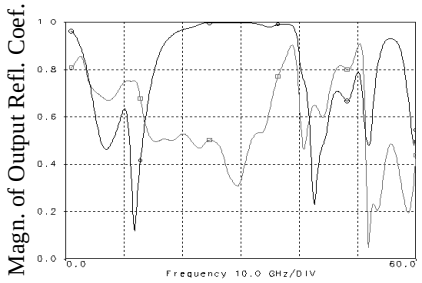

(a)

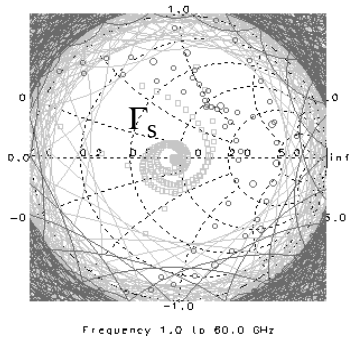

(b)

Fig. 13. (a) Reflection coefficient at the output of the first and second stage when a 50 Ω load is connected at the input. (b) The input stability circles define the region of the source reflection coefficient Γ_G for which the amplifier remains stable. The small squares are the center of the circles.

used to reduce the minimum noise figure of the transistor and improve the input VSWR. The achieved noise figure of the design including the noise generated in the lossy microstrips is within 0.5 dB from the minimum noise figure of the transistor used, the gain is 15 dB flat within 1 dB, and the maximum input VSWR is 3. The design was tested for stability and the regions of source and load impedances for which the design remains stable were found.

Appendix: Simulator Transistor Model

A fairly complete small-signal model of the GaAs MESFET transistor used, is shown in Fig. 14. Although this can be easily realized with the library model FET2 of HP EEsof, the FET2 model does not include noise generators. Unfortunately the models that provide noise generators do not include some significant components of the model of Fig. 14, such as the output impedance components C_{ds} and R_{ds}, and the capacitances C_{gd} and C_{dc}. These models are unreliable for gain simulation, since for example the infinite output impedance would provide infinite available gain. To be able to optimize simultaneously for the gain and

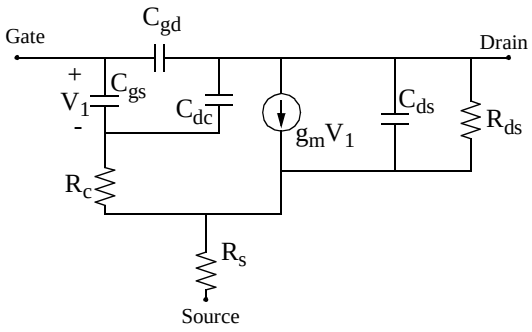

Fig. 14. A fairly complete small signal model for the GaAs MESFET transistor.

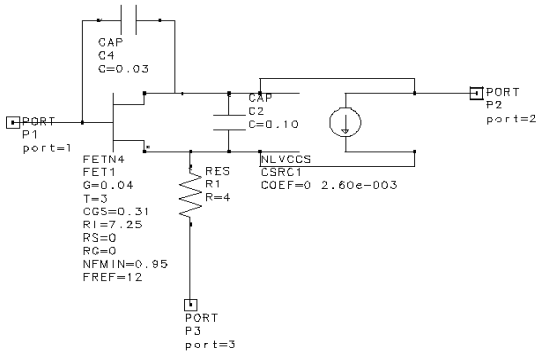

Fig. 15. Modification of the FETN4 model, to include some more parasitic components and make it appropriate for simultaneous noise and gain simulation.

noise figure of our amplifier, the library noise model FETN4 was used, which implements Podell's noise model [6] but it was extended with additional external components as shown in Fig. 15 to make it resemble the model of Fig. 14. The internal R_s of the model was set to zero to make the internal source node available and enable the connection of R_{ds} and C_{ds}, and R_s was then added externaly. Since R_{ds} is not a physical resistor and does not generate thermal noise, this noiseless resistor was implemented with an ideal voltage controlled current source. Finally capacitor C_{dc} was not included in the model, since the common node of C_{gs} and R_c is not an available terminal, but this omission was found not to introduce significant inaccuracy in our simulations. The minimum noise figure of this new extended transistor was simulated and is shown in Fig. 3(b).

References

[1] R. E. Lehman, D. D. Heston, *X-Band Monolithic Series*

Feedback LNA, Texas Instruments, class handout.

[2] S. Ramo, J. R. Whinnery, and T. Van Duzer, *Fields and Waves in Communication Electronics*, Wiley, 1984.

[3] G. D. Vendelin, A. M. Pavio, and U. L. Rohde, *Microwave Circuit Design Using Linear and Nonlinear Techniques*, Wiley, 1990.

[4] H. Statz, H. Haus, and R. Pucel, *Noise Characteristics of Gallium Arsenide Field-Effect Transistors*, IEEE Transactions on Electron Devices, Vol. SC-11, April 1976, pp.243-255.

[5] D. M. Pozar, Microwave Engineering, Second Edition, Wiley, 1998.

[6] A. Podell, A Functional GaAs FET Noise Model, IEEE Transactions Electron Devices, Vol. ED-28, No.5, May 1981, pp. 511-517.